

# How to find long narrow-band gravitational wave transients with unknown frequency evolution?

**Péter Raffai, Zsolt Frei**

Institute of Physics, Eötvös University, Pázmány P. s. 1/A, 1117 Budapest, Hungary

**Zsuzsa Márka, Szabolcs Márka**

Columbia University, Pupin Laboratories, New York, NY 10027

## **Abstract.**

We present two general methods, the so-called Locust and the generalized Hough algorithm, to search for narrow-band signals of moderate frequency evolution and limited duration in datastreams of gravitational wave detectors. Some models of long gamma ray bursts (e.g. van Putten, 2004) predict narrow-band gravitational wave burst signals of limited duration emitted during the gamma ray burst event. These type of signals give rise to curling traces of local maxima in the time-frequency space that can be recovered via image processing methods (Locust and Hough). Tests of the algorithms in the context of the van Putten model were carried out using injected simulated signals into gaussian white noise and also into LIGO-like data. The Locust algorithm has the relative advantage of having higher speed and better general sensitivity, however, the generalized Hough algorithm is more tolerant of trace discontinuities. Combination of the two algorithms increases search robustness and sensitivity at the price of execution speed.

Submitted to: *Class. Quantum Grav.*

PACS numbers: 04.80.Nn, 07.05.Kf, 95.85.Sz

## 1. Introduction

Narrow-band gravitational wave (GW) bursts are one of the types of signals that are expected to be detectable by ground-based interferometric detectors [1], such as LIGO [2, 3], VIRGO [4], TAMA300 [5], and GEO600 [6]. In this paper we examine methods capable of detecting these kind of signals, having unknown frequency evolution and limited duration. Other methods used so far to search for signals with similar characteristics include the tracksearch method [7, 8], the HHT algorithm [9], and methods based on clustering algorithms [10]. In this paper we provide description and test results for two algorithms that are different and independent from these previously used search methods. We will illustrate the two techniques through a plausible astrophysical prediction.

Gravitational waves are expected to be emitted during long gamma-ray burst events, lasting for  $\sim 2 - 100$  s [11, 12, 13, 14, 15]. An alternative model of long gamma ray bursts [16, 17] (GRBs) predicts narrow-band gravitational wave emission lasting for a few tens of seconds during the GBR event, instead of a short transient. The model assumes the source of the radiation to be a magnetically interacting system of a rapidly rotating Kerr black hole surrounded by a uniformly magnetized rotating torus and a remnant stellar envelope. A significant portion of the GRB's energy is emitted by the torus in form of GW radiation. The model predicts the emission of  $T \simeq 90$  s long GW signal for  $7M_{\odot}$  mass black hole, corresponding to the lifetime of the black hole spin. Event rate is predicted to be  $\sim 1$  per year within a distance of 100 Mpc. Nominal frequency of the GW signal is predicted to be around  $f_{GW} \simeq 500$  Hz and scales as

$$f_{GW} \simeq 500Hz \left( \frac{\eta}{0.1} \right) \left( \frac{7M_{\odot}}{M_H} \right), \quad (1)$$

where  $M_H$  is the mass of the Kerr black hole, and  $\eta$  is the ratio of angular velocities of the torus and the Kerr black hole. However, the GW signal frequency is expected to vary slowly with time by a total variation within signal duration of  $\lesssim 10\%$ .

The rotation of the torus around the black hole can be modulated by a precessing motion (Lense-Thirring precession, [18]) that cause an amplitude modulation on the GW signal as well. Angular velocity of this precession is typically around  $\simeq 10\%$  of the angular velocity of the rotating motion of the torus.

GW signal features proposed in this model will be used to illustrate the strengths and limitations of the search methods. For timescales of a few tens of seconds long-term variations, such as tidal effects, rotation of the Earth, motion of the Earth around the Sun, etc, do not appreciably affect the signal. The restriction we impose on the frequency evolution of the function representing a signal is the slow variance of frequency with time.

We present two algorithms ("Locust" and generalized "Hough") that are capable of searching for narrow-band signals, in general. The Locust algorithm uses local wandering, while the Hough algorithm implements the Hough transformation method [19], while providing a generalization such that polynomial curves, not just straight lines, can be fitted. While tests of the methods were carried out using

characteristic signal forms, durations and frequency drifts predicted by the van Putten model of GRBs, we would like to point out that in principle both methods require minimal assumptions about the GW waveform beyond its duration, relatively narrow frequency content and frequency evolution describable with polynomials.

We give a description of the two algorithms as applied in a single detector datastream process, and results of corresponding sensitivity tests in sec.2 and sec.3, respectively. Test results for multiple datastream processing are presented in sec.4.

## 2. Search Method

The pipeline starts with filtering a finite stretch of input data. Then we create a spectrogram of the data stretch by applying discrete Fourier-transformation. The spectrogram is then flattened by normalizing each of its rows separately. Finally, one or both of the image processing methods (Locust and the generalized Hough method) is applied to find traces of local maxima corresponding to signals. In this section a detailed description of each step of the pipeline from filtering to the image processing methods is given.

### 2.1. Transformation of Data into Time-Frequency Space

First the time-amplitude data stream of a single gravitational wave detector is divided into  $T_{seg}$  second long 50% overlapping segments. Taking the van Putten model as a basis, we chose  $T_{seg}$  to be  $T_{seg} = 10$  s, so the amount of overlap is equal to  $T_{seg}/2 = 5$  s. Such segment length provides reasonable search resolution while being a significant fraction of the tens of seconds duration of the long gamma ray burst signals predicted by the model. However, parameter  $T_{seg}$  is to be optimized if faster frequency evolution or significantly different signal duration is expected.

*2.1.1. Filtering* Filtering of input data with respect to the LIGO detectors' spectral sensitivity [20] is performed (IIR, Butterworth bandpass filter in the 80 – 2000 Hz range). At certain frequencies narrow "insensitivity" peaks (power lines, violin mode of mirror suspension, calibration lines, etc.) appear in the spectral sensitivity curve of LIGO detectors which are also eliminated by notch filtering in the time-domain. Filtering in the time domain has the advantage of enabling us to cut out only the narrow peaks from the spectrum without touching the wider frequency environment of Fourier transformation bins and mitigate energy bleeding into other frequency bins.

All filtering procedures were performed via zero-phase means [21] in order to facilitate coherent processing afterwards. Finally  $T_{trans} = 2.5$  s long segments (based on numerical studies of filters) were cut off from the beginning and end of the originally  $T_{seg} = 10$  s long data segment to remove filter transients, leaving  $T = 5$  s for further processing.

*2.1.2. Discrete Fourier-transformation* After filtering, a discrete Fourier-transformation is used to transform the time-amplitude sample into a two-dimensional time-frequency space. In the transform process a Tukey window [22] is used, where the ratio of taper to constant sections is 0.5. The size of the window was chosen to be 2048 ticks, which for a sampling rate of  $Fs = 16384 \text{ Hz}$  provides a frequency resolution of  $8 \text{ Hz/bin}$  and time resolution of  $0.1 \text{ s/bin}$ . The reason for choosing such resolution in tests adapted to the van Putten model is explained in sec.3. However for other type of searched signals, frequency and time resolution (as well as  $T_{seg}$  can be optimized to expected characteristic properties (i.e. duration, frequency evolution) of searched signals.

The sample is split into overlapping sections of size equal to the size of the window: the overlap between neighboring segments is  $1/4$  of the window size. After the transformation of the data, only the relevant frequency range that is compatible with the range of the bandpass filter (i.e.  $80 - 2048 \text{ Hz}$ ) is processed further.

In case of processing the data stream of a single detector, we take the absolute value of every element in the resulting matrix of Fourier-coefficients. As a result, we get a matrix of non-negative real elements. The rows of this matrix represent the frequency while columns the time axis of the Fourier-space.

*2.1.3. Spectrum Flattening* Filtering and detector response presents the data such that certain frequency regions get overemphasized or deemphasized. This effect is transferred into the Fourier-coefficient matrix, thus its rows need to be normalized with respect to each other. Hereafter, we refer to this normalization process as "flattening". This procedure produces similar results to "whitening" generally applied during the filtering phase for other methods [23].

If a filtered data sample only consists of random noise and does not contain contributions from a real signal, then we empirically found the magnitude of the Fourier-coefficients in each row to be well described by a gamma distribution. In the case of signal presence in the data, the resulting distribution of coefficients is altered from this gamma distribution in the range of the highest values.

One can identify segments of data that are nearby in time, and are therefore expected to have similar frequency content, but no signal. We apply the gamma distribution fit to rows of spectrograms that belong to such data segments. Therefore the average and sigma that is used in the flattening process are deduced from different spectrograms that are shifted in time compared to the spectrogram to be flattened. This permits the flattening procedure to suppress constant spectrum lines, but not affect actual signals.

The flattening process then continues with the subtraction of this average from every element of the row and the division of the row by sigma. This procedure essentially takes away the fraction of power in the given frequency bin that is associated with the "average" noise (noise power removal). This process is done for every row of the matrix separately.

There is a chance for some elements of the matrix to become negative after the

subtraction of the mean in the flattening process. This can only happen for elements in a row with the lowest values, that surely correspond only to noise and does not contain contributions from the signal. To save running time, we cut out all negative elements of the flattened matrix by replacing their value with zero.

In this paper from now on we will refer to the resulting flattened Fourier-coefficient matrix consisting of only non-negative elements as "spectrogram".

## 2.2. Image Processing Algorithms

A generalized narrow-band signal in the input data will manifest itself as a trace consisting of a chain of local maxima in the time-frequency space. This can be described as a polynomial function of time. Our goal is to find and identify these traces in the noisy background. We treat the two-dimensional time-frequency space as a grayscale image, for which the shade of a pixel is proportional to the magnitude of the corresponding matrix element (i.e. excess energy), thus signal search task is converted into an image processing problem. We have used two independent algorithms in image analysis: the so called Locust algorithm (conceived by us), and a method based on the generalized Hough-transform.

*2.2.1. The Locust Algorithm* The method is based on a gradient driven wandering. Traces of local maxima to be identified in the spectrogram image of the input data consists of loosely connected chains of non-negative elements.

The starting point of the search is always the global maximum of the processed spectrogram. The value and coordinates of this global maximum are stored, and the value is reduced to zero immediately. We then search for the maximum in the local environment of this starting point, described by  $n \times m$  time-frequency bins heading forward in time. The value and coordinates are stored and the value is reduced to zero again. Coordinates of this local maximum is treated as the new starting point of the search. The following local maxima are then searched, stored, and reduced to zero similar way, until we reach the edge of the spectrogram or at any time the maximum in a local environment is found to be zero. The described wandering is then repeated the same way, but heading backward in time from the original starting point (i.e. the former global maximum of the spectrogram).

Such forward-backward path pairs obtained by the search represents one trace of local maxima we are looking for. If the ratio of the sum over the number of elements in the integral for a given trace exceeds the value of a preset threshold, the search results in an alarm and the properties of the trace are saved. The Locust search then continues from the next global maximum of the matrix, until every element of the matrix are reduced to zero.

The final step of the Locust search visualizes saved traces, first separately, then together in one image. All trace elements are added to a null-matrix of same size as the spectrogram, and a polynomial curve of given order is fitted to elements of this resulting

matrix. The parameters of the polynomial fit are determined via minimization of the distance of the fit from the trace pixel element positions, weighted by the actual grayscale shade (that is significance of the given time-frequency bin) of each pixel. Knowing the parameters of the polynomial curve having the best fit to the traces allows us to give an estimate on the properties of the GW source in the context of the applied model of long GRBs.

An example for resulting images of Locust search is shown in fig.(1).

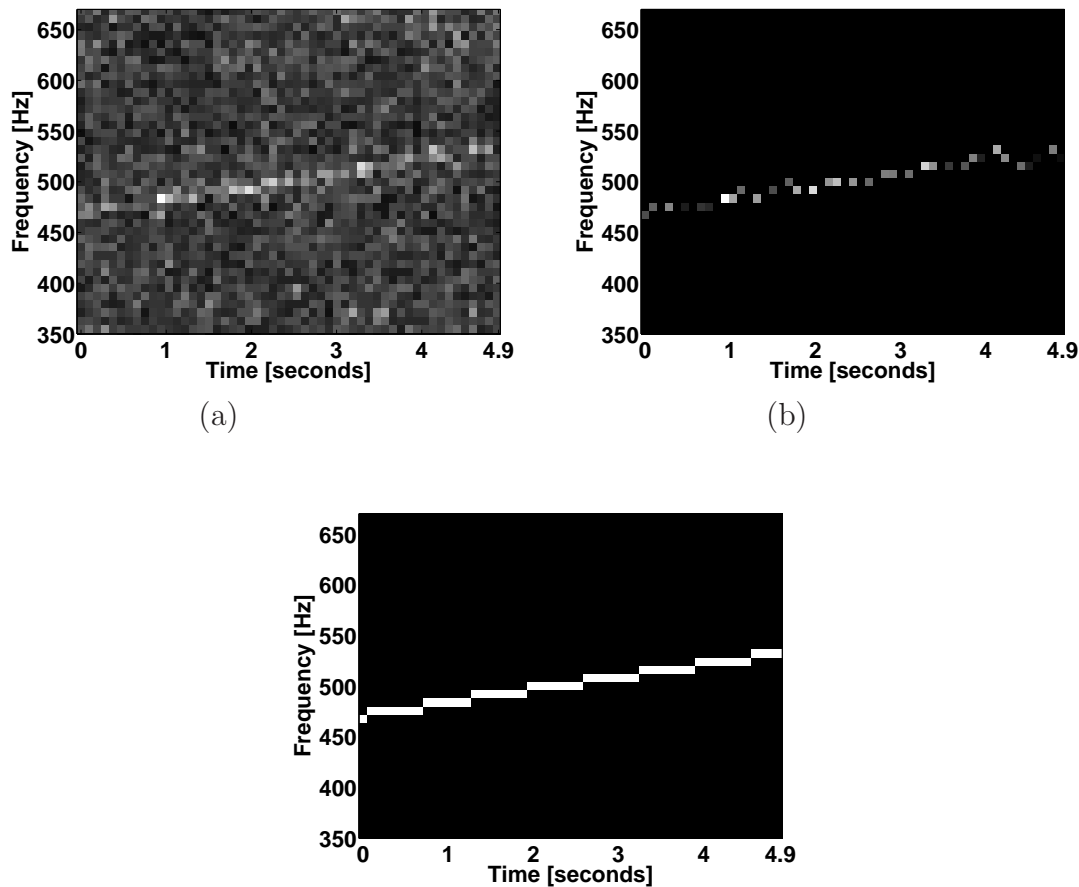


**Figure 1.** Pre-processed spectrogram of input data in the local frequency environment of injected signal (a). Plot of a trace satisfying the alarm requirements of the Locust method (b). A second order polynomial curve fitted to the above trace found by Locust method (c).

### 2.3. The Generalized Hough Algorithm

This is a generalization of the Hough-transform method [19] and is based on polynomial curve fitting to a trace of local maxima instead of the traditional line. First a dimension parameter ( $D$ ) is chosen representing the dimension of the space of polynomial parameters. In most implementations of the Hough transform only linear fits are considered ( $D = 2$ ). We shall consider higher order polynomials. For a given dimension

parameter,  $D$  number of positive elements from the spectrogram are selected and a polynomial curve of  $D - 1$  order is fitted to them. This procedure continues for other  $D$  number of positive elements from the spectrogram until every combination of positive elements are taken into account.

This process results in an 'output matrix' of  $D$  columns and  $\binom{N}{D}$  - the number of different combinations - rows, where  $N$  is the total number of positive elements in the matrix. Each row of this 'output matrix' contain polynomial fit parameters that describe a position vector of a single datapoint in the "Hough space" (essentially a  $D$ -dimensional polynomial parameter space). If a signal is present in the input data, and its frequency evolution can be described by a polynomial function of order  $D - 1$ , the resulting data points in the "Hough space" have an extremely high density within a small parameter region. To identify this high density region, we collect data points in histogram bins for each parameter, and look for the bin that contains the most data points. Binsize was chosen to be such as to minimize the probability for multiple datapoints to be in one bin for an approximately homogeneous density distribution (i.e. in the absence of a signal in input data), while still get an appreciable resolution for the histogram. We choose final parameters of the polynomial (and thus the best fit to the signal trace) to be equal to the components of the position vector that points to the closest datapoint to the center of mass of the bin with the highest number of datapoints. The Hough search process then results in an alarm if the ratio of the sum of Fourier-coefficients in the 1 bin local frequency environment along the found polynomial trace, over the number of these coefficients, exceed a predefined threshold.

An example for the binned parameter space in the proximity of the density maximum is shown in fig.(2).

Execution time of the Hough process is proportional to  $N^D$ . In order to save running time, we can reduce  $N$ , the number of positive elements in the spectrogram. Because Fourier-coefficients with the highest values have the highest probability to belong to a trace corresponding to a potential signal, we keep a certain number of elements with the highest value and reduce value of the rest of the elements to zero. In our tests, we chose this number to be 15. The number of elements to be left untouched was and can be optimized to a limit that our false alarm rate and execution speed tolerance requirement allows.

#### 2.4. Comparison of Locust and Hough algorithms

The characteristic features of traces for which Locust and Hough methods are the most sensitive differ in many aspects.

The condition for alarm in the Locust method are independent from the length of the trace and all traces of a spectrogram satisfying alarm conditions are treated as parts of one trace with discontinuities. However, the detection efficiency for the Locust algorithm drops if the trace corresponding to a signal has significant discontinuities beyond the  $\Delta f \times \Delta t$  size of the local environment of the search. In that case the Locust

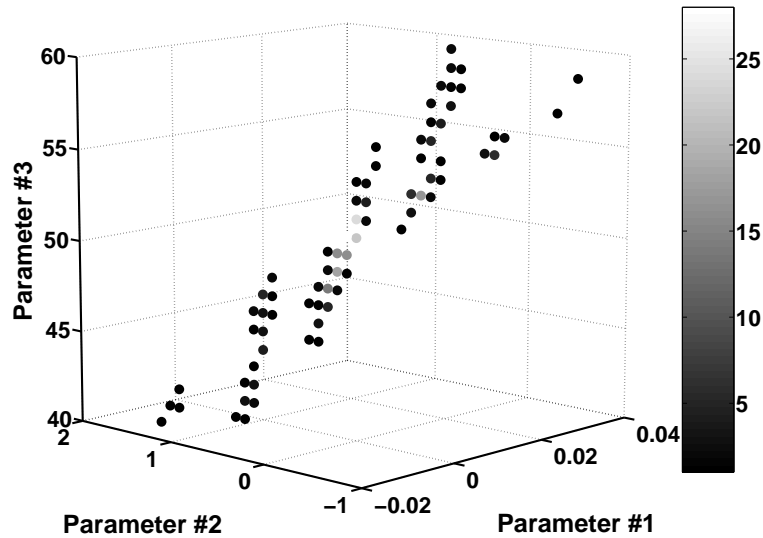


**Figure 2.** Three dimensional binned Hough parameter space (corresponding to second order polynomials fitted to traces of local maxima in the spectrogram), in proximity of the density maximum. Shade of markers represent the number of datapoints in the appropriate bins. Parameters of the best fit are chosen to correspond to the closest datapoint to the center of mass of the bin with the highest number of datapoints.

search chooses a maximum from the noise background and might continue the process by following local noise maxima. Thus the final trace may not reach the threshold level for alarm even if it contains segmental contributions of a real signal. This effect is more likely at low signal-to-noise ratios, and can be reduced by optimizing the size of the local environment applied in the Locust maximum search to the expected signal-to-noise ratios.

Compared to the Hough method, the Locust method has the relative advantage of higher execution speed and its performance in principle is less dependent from the order of the polynomial to be fitted to the identified traces (somewhat independent from the signal waveform).

Detection efficiency of the Hough search process is less dependent on trace discontinuities, however it is highly dependent on the order of the polynomial to be fit (D-1). Increasing D leads to an exponentially greater computational time. This can be partially compensated by decreasing the number of non-zero elements used in the Hough transform, which saves execution time, however decreases detection probability at the same time.

Because of their differing response to the choice of signal trace polynomial fit and to trace discontinuities, a combination of the two independent methods (Locust and generalized Hough) in one search process can lead to higher sensitivity with a cost of greater computational time. The easiest way to combine the two algorithms in one process is to apply both of them in parallel on the same datastream, and to take the union of their outputs.

### 3. ROC-tests

The sensitivity of our search methods was tested by finding the detection probability versus false alarm rate (i.e. the receiver operating curve or ROC) for injected signals into simulated noise.

We have completed our tests for two types of noise; gaussian white noise and a LIGO-like data with basic statistical characteristics (e.g. amplitude distribution, spectral compatibility) of LIGO 4 km detectors during the 4th science run [24]. To calculate the detection probabilities and false alarm rates, we used 500 samples from gaussian and 250 samples from LIGO-like noise, all are 10 s long and overlapping as described before in sec.2.

Gravitational wave signals ( $h(t)$ ) can be expressed as linear combinations of signals of two independent polarizations:

$$h(t) = F_+ h_+(t) + F_\times h_\times(t) \quad (2)$$

where  $F_+$  and  $F_\times$  are linear coefficients dependent on the detector's directional sensitivity characteristics and the position of the source in the sky.

In the van Putten model [16]  $h_+(t)$  and  $h_\times(t)$  are expressed as

$$h_+(t) = A \times (1 + l(t)^2) \times \cos(2 \times \Omega_T(t) \times t) \quad (3)$$

and

$$h_\times(t) = -2 \times A \times l(t) \times \sin(2 \times \Omega_T(t) \times t). \quad (4)$$

In these expressions  $A$  is the amplitude of the GW signal while the time-dependent geometrical factor,  $l(t)$ , and the angular velocity of the torus in the van Putten model [16],  $\Omega_T(t)$ , are functions of time:

$$l(t) = B \times \cos(\Omega_{LT}(t) \times t) + D \quad (5)$$

where  $\Omega_{LT}(t)$  is the angular velocity of the potential Lense-Thirring precession of the torus, while  $B$ ,  $D$  are other variables dependent on the properties of the source and parameters of its motion (see [16, 15] for details).

In general,  $\Omega_T$  can be any kind of continuous function of time, but in our analysis the simplest but still not trivial case of second order polynomials were considered. In our tests, function representing  $\Omega_T(t)$  was chosen such to cover the  $\pm 10\%$  range of  $f_{\text{GW}} \simeq 500 \text{ Hz}$  (see sec.1) with the resulting frequency of the injected GW signal,  $\Omega_T/\pi$ . Since our analysis is carried out in time-frequency space and the functions that describe the frequency evolution of GW signals are the same for both polarizations, search sensitivity and test results are the same for signal functions of both kind. For this reason, the results are given only for  $h_+(t)$ .

As it is seen in eq.(5), a possible Lense-Thirring precession of the torus might modulate the van Putten signal with a cosine function of frequency  $\Omega_{LT}$ . This causes sidebands to appear in the spectrum of the signal at frequencies  $2\Omega_T + \Omega_{LT}$  and  $2\Omega_T - \Omega_{LT}$ . According to predictions of the van Putten model [16],  $\Omega_{LT}$  typically

does not exceed the nominal value of  $\simeq 0.1\Omega_T$  [16]. We chose frequency resolution of our demonstration (8 Hz/bin) such that modulation sidebands usually do not appear in separate frequency bins from the main trace of the signal. Possible slight broadening of the main trace however can be handled by both Locust and Hough algorithms.

The Locust algorithm results with an alarm, if the ratio of the integral and the number of elements of a trace exceeds a given threshold,  $C$ . In case of the Hough method, the same ratio is calculated and compared to a predefined threshold,  $C$ , but integration is carried out for the 1 bin local frequency environment along the polynomial curve found by method.

To map ROC characteristics of a method, one first needs to explore the detection probability and the false alarm rate as a function of threshold  $C$ . Using gaussian white noise and LIGO-like noise samples without injections (all going through identical processing described in section 2.1), we applied the Locust and Hough methods. The distribution results then directly gives us the false alarm rate (FAR) as a function of  $C$ . We follow the same method, but with injection of van Putten type signals (eq.(3)) to find the detection probability for the same  $C$  threshold values. Each point on the ROC curves is then produced by identifying the  $C$  threshold value for a given false alarm rate from the FAR vs.  $C$  empirical curve and then finding the detection probability corresponding to the same  $C$  threshold using the detection probability vs.  $C$  curve. At extremely low FARs and detection probabilities linear extrapolation to the log-log tail of the empirical FAR (or detection probability) vs.  $C$  curves was used.

The resulting ROC-curves of the Locust and Hough methods, for four different signal root sum square amplitudes (i.e.  $hrss = \sqrt{\int h(t)^2 dt}$ , [25]) in the  $hrss = 6.3 \times 10^{-21} - 2.1 \times 10^{-20} 1/\sqrt{Hz}$  range are given in fig.(3). The corresponding LIGO-like data noise sensitivity in the 400-600 Hz region (corresponding to the injected van Putten type signal's frequency content) is  $\sim 3.8 \times 10^{-22} 1/\sqrt{Hz}$ . For gaussian white noise data (mean=0, sigma=1) the injected hrss-s range is  $6.6 \times 10^{-2} - 2.2 \times 10^{-1} 1/\sqrt{Hz}$ .

#### 4. Processing datastreams of multiple detectors

As an obvious generalization, we can increase search sensitivity via coherent use of data streams of multiple interferometers, and process the resulting single stream with the Locust and Hough methods. If the time delay between the realization of the same signal in different data streams is well known, the data streams can be synchronized by shifting one of the streams relatively to the other by the known delay. Additionally the detectors' orientation with respect to each other and the proposed source direction (i.e. the antenna factors) can also be taken into account.

We will illustrate the simplest case where sky position is known (optimal) and the detectors are aligned. After the data are synchronized, they are processed the same way as described in section 2.1 to the step of discrete Fourier-transformation resulting in the matrix of complex Fourier-coefficients. The correlation process is carried out on these complex matrices. Let us denote these two matrices by  $s_1$  and  $s_2$  respectively. The

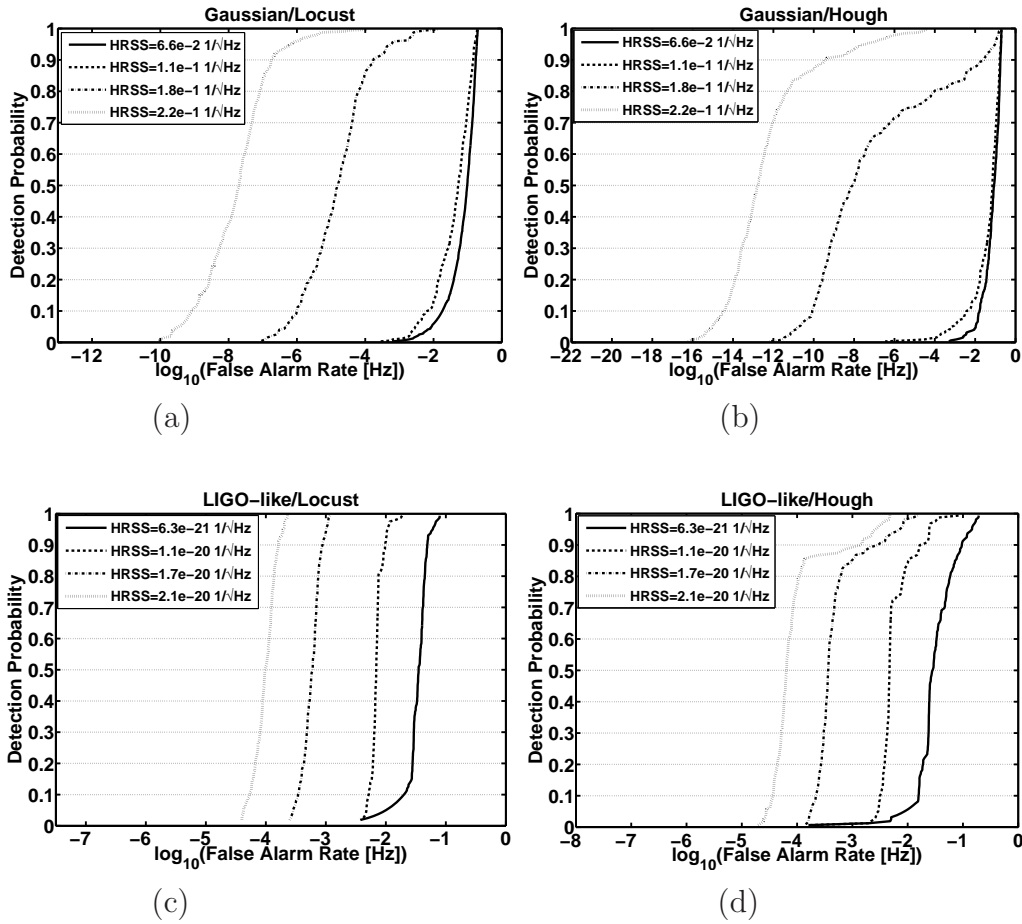


**Figure 3.** ROC curves of single datastream searches. a:white noise/Locust, b:white noise/Hough, c:modified LIGO/Locust, d:modified LIGO/Hough.

correlation matrix,  $c$ , can be calculated in time-frequency space, using the following expression:

$$c(m, n) = \sqrt{\frac{s_1(m, n) s_2^*(m, n) + s_1^*(m, n) s_2(m, n)}{2}} \quad (6)$$

where  $s_i^*$  is the complex conjugate of  $s_i$ . Note, that if  $s_1 = s_2 = s$  (i.e. single detector case),  $c$  is the absolute value of the complex  $s$  matrix, thus we get back the input for the single datastream process.

In principle true GW signals present in the coherent datastreams are correlated and thus give rise to positive values in the correlation matrix. On the other hand, noises in the two datastreams are uncorrelated and the corresponding correlation coefficients are randomly distributed around zero. Therefore negative values and the lower portion of the positive values in the distribution of the correlation coefficients can be attributed to noise and can be changed to the zero level during image processing to speed up processing.

The resulting ROC-curves of the Locust and Hough methods in case of a multiple

datastream search and for the same injected signals as for the single detector case are given in fig.(4).

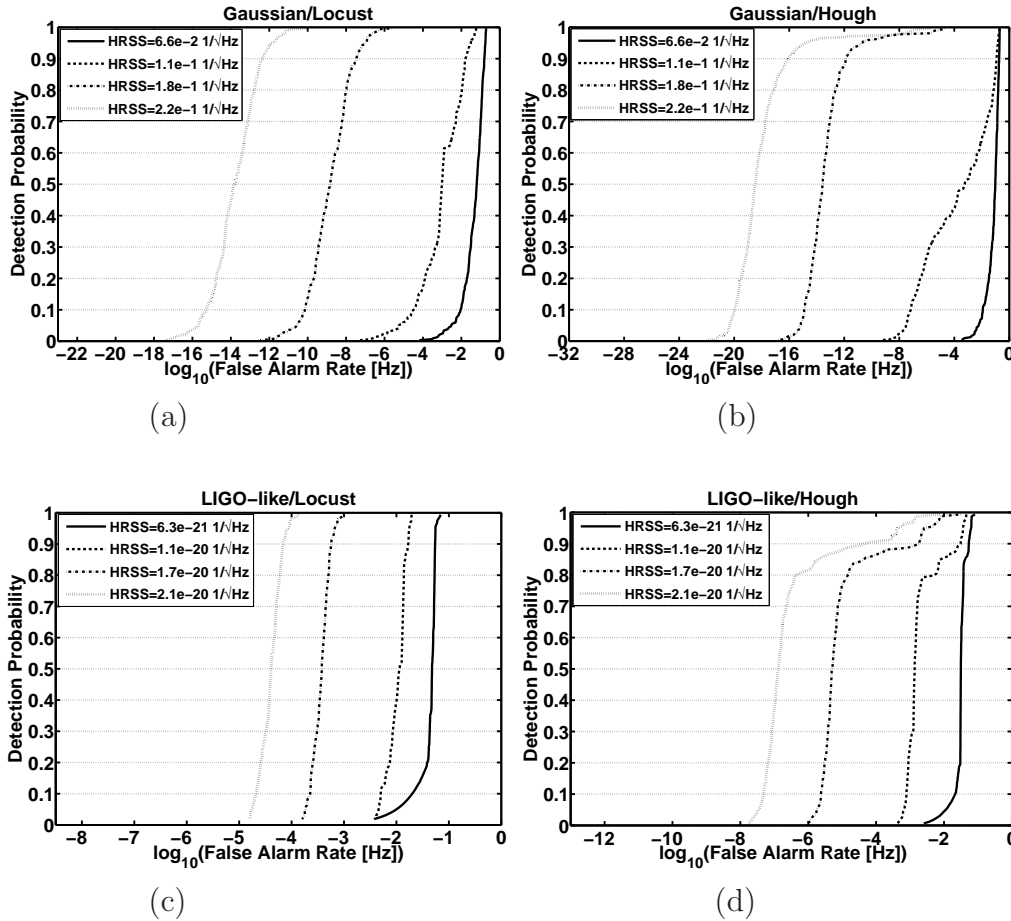


**Figure 4.** ROC curves of multiple datastream searches for two coaligned and equal sensitivity detectors. a:white noise/Locust, b:white noise/Hough, c:modified LIGO/Locust, d:modified LIGO/Hough.

## 5. Discussion of ROC test results

Theoretical modeling of sensitivity results is beyond the scope of this technical paper. However, ROC curves characterizing the sensitivity of Locust and Hough algorithms are statistical in nature and at this point practically can be measured. Thus in this section, we emphasize only some qualitative issues of sensitivity analysis and ROC characteristics.

As seen in section 2.2.1 the Locust algorithm identifies traces by following the path of local maxima in the spectrogram, more likely to correspond to a signal. This method is not dependent on the expected shape of a continuous trace in the spectrogram, however finding a local maximum that does not have contribution from a signal might lead the

algorithm to follow a wrong path, collecting power from only pure noise, or pure noise together with signal contributions.

The Hough algorithm uses more global characteristics of a signal trace, it is more robust to local signal characteristics. It takes advantage of a known (or expected) function describing the frequency evolution of the signal with time. In case the null-hypothesis on the order of polynomial describing frequency evolution is correct, even long discontinuities in signal trace will not decrease the sensitivity of the Hough method as long as signal elements are located along the appropriate polynomial curve.

In our tests, frequency of injected signals is chosen to be a second order polynomial of time (see section 3), and the Hough method is using the appropriate dimension parameter,  $D$  (right polynomial order in fit). Thus in this case, the Hough method takes advantage of the additional information about the signal, while the Locust does not, resulting with better sensitivity for the Hough method than for the Locust method. However in general, if frequency evolution is totally unknown and/or cannot be described with a polynomial function, we expect the Locust algorithm to be more sensitive than the Hough method (see figure 3 and 4).

The cross-correlation of multiple datastreams in time-frequency space is practically equivalent to a normalized multiplication of the spectrograms consisting of correlated signal and uncorrelated noise contributions. This step suppresses noise contributions, increasing the contrast between a signal trace and the noise background. If the contrast between noise and signal contributions is increased, both methods get more sensitive (as seen in figure 4).

The Hough search method applies a cut in the spectrogram, leaving only the  $N$  highest elements of the spectrogram for further processing. The Locust method does not apply this kind of a cut. The cross-correlation surely increase the number of signal contributions among the highest  $N$  elements remaining after the cut in the Hough method. However, the increase of the trace contrast (increases its probability, but) does not guarantee, that the relatively higher signal contribution values will finally be located in their local "Locust" environment of each other. So the cross-correlation of multiple datastreams should affect sensitivity results for the Hough method more, than the sensitivity results for the Locust method. This is of course only true, if for the single detector case, the highest  $N$  elements left for Hough search is a mixed set of signal and noise spectrogram elements. If all  $N$  element is from noise (signal HRSS too low), or if all  $N$  element is from a signal (signal HRSS too high), the additional increase of Hough method's sensitivity relative to the Locust method's increased sensitivity does not appear in the multiple detector case (see figure 4).

## 6. Conclusion

We have examined two methods to search for narrow-band gravitational wave signals in datastreams of interferometric gravitational wave detectors. Both algorithms are applied in time-frequency space. The so called Locust algorithm uses local wandering,

searching for traces of local maxima in spectrogram of input data. The Hough method is based on a generalized Hough transform, capable of recognizing polynomial curve-like features in the noisy environment of a spectrogram.

Performance measures of these algorithms are illustrated in the context of the van Putten model of long gamma ray bursts and using gaussian white noise and also LIGO-like noise. We characterized the search sensitivity of the two algorithms by mapping Receiver Operating Curves for various signal amplitudes.

As the Locust algorithm uses local wandering, the Hough algorithm has the relative advantage of higher robustness to trace discontinuities. The Locust algorithm is significantly faster and is more general in the sense that it does not require any pre-assumptions on the function describing time evolution of signal frequency. Applying the two algorithms in parallel in one search process provides an opportunity to overcome both above mentioned relative disadvantages for a price of execution speed.

Search methods described in this paper in principle are capable of processing both single and multiple datastreams of gravitational wave detectors. Using the correlation matrix in further steps of search process increases search sensitivity of our methods.

## 7. Acknowledgements

The authors are grateful for the support of the United States National Science Foundation under cooperative agreement PHY-04-57528, Columbia University in the City of New York and Eötvös University in Hungary. We are grateful to the LIGO collaboration for their support and in particular to P. Shawhan.

This paper has been assigned LIGO Document Number LIGO-P070025-00-Z.

## 8. References

- [1] S.A. Hughes, S. Marka, P.L. Bender and C.J. Hogan, Proceedings of the 2001 Snowmass Meeting **eConfC010630**, P402 (2001).
- [2] B. Abbott et al., Nuclear Instruments and Methods in Physics Research A **517**, 154 (2004).
- [3] D. Sigg and the LIGO Scientific Collaboration, Classical and Quantum Gravity **23**, 51 (2006).
- [4] F. Acernese et al., Classical and Quantum Gravity **23**, S63 (2006).
- [5] R. Takahashi et al., Classical and Quantum Gravity **21**, S403 (2004).
- [6] H. Lück et al., Classical and Quantum Gravity **23**, S71 (2006).
- [7] W.G. Anderson and R. Balasubramanian, Physical Review D **60**, 102001 (1999).
- [8] C. Torres and W.G. Anderson, Classical and Quantum Gravity **22**, S1169 (2005).
- [9] J.B. Camp, J.K. Cannizzo and K. Numata, Physical Review D **75**, 061101 (2007).
- [10] R. Khan and S. Chatterji, Classical and Quantum Gravity, 11th GWDAW Conference Proceedings (2007).
- [11] C. Kouveliotou et al., Astrophysical Journal **413**, L101 (1993).
- [12] S. Mohanty et al., Classical and Quantum Gravity **21**, S1831 (2004).
- [13] S. Marka and L. Matone, AIP Conference Proceedings **836**, 605 (2006).
- [14] M.H.P.M. van Putten, Astrophysical Journal Letters **575**, L71 (2002).
- [15] M.H.P.M. van Putten, "Gravitational Radiation, Luminous Black Holes and Gamma-Ray Burst Supernovae", Cambridge University Press (2005).

- [16] M.H.P.M. van Putten, A. Levinson, H.K. Lee, T. Regimbau, M. Punturo and G.M. Harry, *Physical Review D* **69**, 044007 (2004).
- [17] O. Bromberg, A. Levinson and M.H.P.M. van Putten, *New Astronomy* **11**, 619 (2006).
- [18] J. Lense and H. Thirring, *Phy. Z.* **19**, 156 (1918).
- [19] P.V.C. Hough, International Conference on High Energy Accelerators and Instrumentation, CERN (1959).
- [20] <http://www.ligo.caltech.edu/docs/G/G060054-00/G060054-00.pdf>
- [21] R.W. Hamming, "Digital Filters", Prentice-Hall (1983).
- [22] F.J. Harris, *Proceedings of the IEEE* **66**, 66 (1978).
- [23] S.K. Chatterji, "The search for gravitational wave bursts in data from the second LIGO science run", PhD dissertation, Massachusetts Institute of Technology (2005).
- [24] D. Sigg, *Classical and Quantum Gravity* **23**, S51 (2006).
- [25] LIGO Scientific Collaboration, *Physical Review D* **72**, 062001 (2005).